Supporting information

Integrating 2D elasticity and elastoplasticity into a multi-stimuli-responsive crystal through phase transitions

Yihang Hou [‡a], Pengpeng Yang [‡b], Jingjing Zhao[a], Jinqiu Fu[a], Chiyi Wang[a], Yuzhong Shi[a], Wei Zhuang[b], Keke Zhang[a,*], Hanjie Ying[b]

[a] Y. Hou, J. Zhao, J. Fu, C. Wang, Y. Shi and Dr. K. Zhang*
Biology+ Joint Research Center, School of Chemical Engineering and Technology, Zhengzhou University
Zhengzhou 450001, China
*E-mail: zhangkeke@zzu.edu.cn

[b] Prof. P. Yang, W. Zhuang and H. Ying
National Engineering Technique Research Center for Biotechnology, State Key Laboratory of Materials-Oriented Chemical Engineering, College of Biotechnology and Pharmaceutical Engineering, Nanjing Tech University
Nanjing 211816, China

Table of Contents

1. Experimental Section

1.1. Materials and crystallization

Isonicotinamide (INA) of analytical grade was purchased from Macklin (I811781-500g). Deionized water was prepared in our laboratory. Vacuum silicone grease was purchased from Great Wall (7501). All the reagents were used without further purification.

Preparation of INA form H single crystals with different habits. Solvent evaporation method was used to crystallize the INA form **H**.[1] We prepared a series of unsaturated aqueous solutions of INA with different concentrations ranging from 0.05-0.3 g ml^{-1} in the beakers at 50 °C, then kept them at room temperature to quickly cool down. Then the clear solution was transferred to the Petri dishes to volatilize the solvent, and INA form **H** crystals with different crystal habits were harvested after one day. The mixture of acicular and rod-like crystals was harvested at 0.1-0.3 g ml^{-1}, where the amount of acicular crystals was more at a solution concentration of 0.2-0.3 g ml^{-1}, and the crystallization of rod-like crystals was preferred below 0.1 g ml^{-1}.

Preparation of INA polymorphs. Single crystal-to-single crystal (SC-SC) transitions of the acicular crystals of INA from form **H** to form **I** were actuated by controlling humidity. In the humidity experiment, an acicular crystal of form **H** was placed in the dryer at 0% RH and ambient temperature, then an acicular crystal of form **I** was obtained after three days. In the temperature experiment, an acicular crystal of form **H** was placed on the surface of a temperature-control stage and heated from ambient temperature to 40 °C or 50 °C quickly in atmosphere with about 30% RH, then an acicular crystal of form **I** (40 °C) or form **II** (50 °C) was obtained after three days. The single crystal of form **II** used for structure determination by single crystal X-ray diffraction (SCXRD) was obtained by cooling crystallization. In this experiment, a saturated aqueous solution at 55 °C of INA was cooled to 25 °C at a rate of 5 °C h^{-1}, then being maintained at 25 °C for one week, and the crystals of form **II** were harvested ultimately.[2]

1.2. Instrumental methods and calculations

Single crystal X-ray diffraction measurements and structural refinement. SCXRD measurements were operated on a Rigaku Saturn 70 CCD diffractometer. The crystals of INA were all kept at 113.15 K during data collection. The structure was solved by Olex2 with the ShelXT structure solution program using Intrinsic Phasing and refined with the ShelXL refinement package using Least Squares minimisation.[3-5] The crystallographic data of forms **H**,

I and **II** has been deposited with Cambridge Crystallographic Data Centre (CCDC), and signed to CCDC codes 2251153, 2251048 and 2251049, respectively.

Powder X-ray diffraction measurements. The powder X-ray diffraction data were collected on a Bruker D8 Advance diffractometer with CuKα radiation (λ = 1.54060 Å). The measurement 2θ ranged from 5 to 40° at a scan rate of 10 ° min^{-1}. All samples tested were ground into powder.

Micro-Raman spectroscopy. The Raman spectra were collected on a Renishaw inVia spectrometer using a 633 nm excitation laser operating at 50 mW. Laser spot on the samples was focused to 2 μm. The measured bent crystals of INA forms were all fixed with tapes at two ends on the glass slides and all samples were single crystals, not powders.

Scanning electron microscope (SEM). The electron microscope images of INA crystals were captured using a Thermo Scientific Phenom Pure G6 Desktop SEM. Single crystal samples were deposited on a carbon stripe and sputtered with gold before being introduced into the instrument. The operating voltage was 5 kV during imaging.

Energy framework calculations. The energy frameworks of INA forms **H**, **I** and **II** were calculated respectively, constructed from pairwise interaction energies considering radius of 3.8 Å between the centroid of INA molecule and another atom of neighboring molecules, based on the B3LYP/6-31G(d, p) level of theory in CrystalExplorer17.5.[6] Thicker cylindrical tubes represent the stronger interactions. The energy cut-off was 5 kJ mol^{-1} and tube size was 100.

2. Results and Discussion

2.1. Crystallographic information

Table S1. Crystallographic and structural refinement parameters of INA forms **H**, **I** and **II**.

Compounds	**Form H**	**Form I**	**Form II**
Empirical formula	$C_6H_8N_2O_2$	$C_6H_6N_2O$	$C_6H_6N_2O$
CCDC code	2251153	2251048	2251049
Formula weight	140.14	122.13	122.13
Temperature/K	113.15	113.15	113.15
Crystal system	monoclinic	monoclinic	monoclinic
Space group	$P2_1/n$	$P2_1/c$	$P2_1/c$
a / Å	7.4163(7)	10.1796(10)	15.7376(19)
b / Å	10.8145(9)	5.7328(6)	8.0174(7)
c / Å	16.6663(15)	10.0248(9)	9.9053(9)
α / °	90	90	90
β / °	93.103(9)	98.126(9)	105.530(11)
γ / °	90	90	90
Volume / Å^3	1334.7(2)	579.15(10)	1204.2(2)
Z	8	4	8
ρ_{calc} / g cm^{-3}	1.395	1.401	1.347
μ / mm^{-1}	0.107	0.1	0.096
F (000)	592	256	512
Crystal size / mm^3	0.13 × 0.1 × 0.08	0.25 × 0.22 × 0.17	0.23 × 0.2 × 0.16
Radiation	MoKα (λ = 0.71073)	MoKα (λ = 0.71073)	MoKα (λ = 0.71073)
2θ range for data collection / °	4.492 to 52.74	4.042 to 52.71	5.374 to 56.558
Index ranges	-9 ≤ h ≤ 9, -13 ≤ k ≤ 13, -1 ≤ l ≤ 20	-12 ≤ h ≤ 12, -7 ≤ k ≤ 7, -12 ≤ l ≤ 12	-20 ≤ h ≤ 20, -10 ≤ k ≤ 10, -12 ≤ l ≤ 13
Reflections collected	2727	5647	11692
Independent reflections	2727	1183	2981
Data/restraints/parameters	2727/0/188	1183/0/83	2981/0/164
Goodness-of-fit on F^2	1.27	1.074	1.059
Final R indexes [I >= 2σ(I)]	R_1 = 0.0770, wR_2 = 0.1522	R_1 = 0.0466, wR_2 = 0.1139	R_1 = 0.0708, wR_2 = 0.1424
Final R indexes [all data]	R_1 = 0.1058, wR_2 = 0.1618	R_1 = 0.0571, wR_2 = 0.1215	R_1 = 0.1248, wR_2 = 0.1696
Largest diff. peak/hole / e Å^{-3}	0.30/-0.37	0.22/-0.22	0.29/-0.23

2.2. Molecular structures, torsion angles and overlays

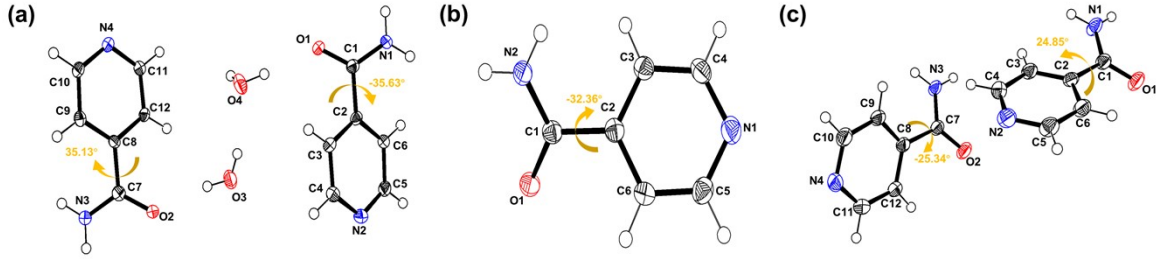

Figure S1. Molecular structures with torsion angles of INA (a) forms **H**, (b) **I** and (c) **II**, showing thermal displacement ellipsoids (drawn at the 50% probability level) with atom numbering labels.

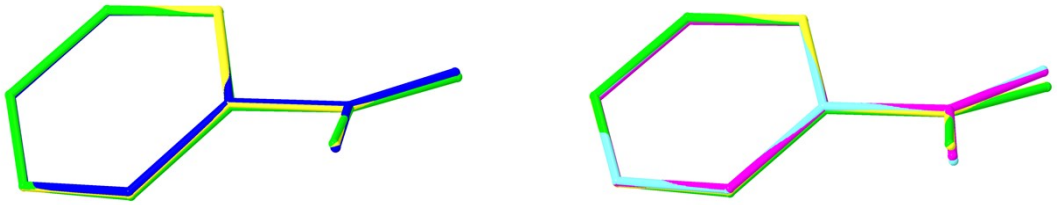

Figure S2. Overlays of the conformations in the crystal structures of INA (left) forms **H** and **I**, (right) forms **H** and **II**. The yellow and green conformations represent INA molecules of form **H**, dark blue for form **I**, purple and nattier blue for form **II**.

Table S2. Torsion Angles of INA forms **H**, **I** and **II**.

Form H					Form I					Form II				
A	**B**	**C**	**D**	**Angle / °**	**A**	**B**	**C**	**D**	**Angle / °**	**A**	**B**	**C**	**D**	**Angle / °**
O1	C1	C2	C3	-33.2(6)	O1	C1	C2	C3	146.96(17)	O1	C1	C2	C3	-153.8(2)
O1	C1	C2	C6	143.9(4)	O1	C1	C2	C6	-30.7(2)	O1	C1	C2	C6	24.2(4)
N1	C1	C2	C3	147.4(4)	N2	C1	C2	C3	-32.3(2)	N1	C1	C2	C3	24.9(4)
N1	C1	C2	C6	-35.6(6)	N2	C1	C2	C6	150.01(17)	N1	C1	C2	C6	-157.1(2)
O2	C7	C8	C9	-144.7(4)						O2	C7	C8	C9	153.2(2)
O2	C7	C8	C12	34.7(6)						O2	C7	C8	C12	-25.3(4)
N3	C7	C8	C9	35.1(6)						N3	C7	C8	C9	-25.3(4)
N3	C7	C8	C12	-145.5(4)						N3	C7	C8	C12	156.1(2)

2.3. Molecular packings and face indexing measurements

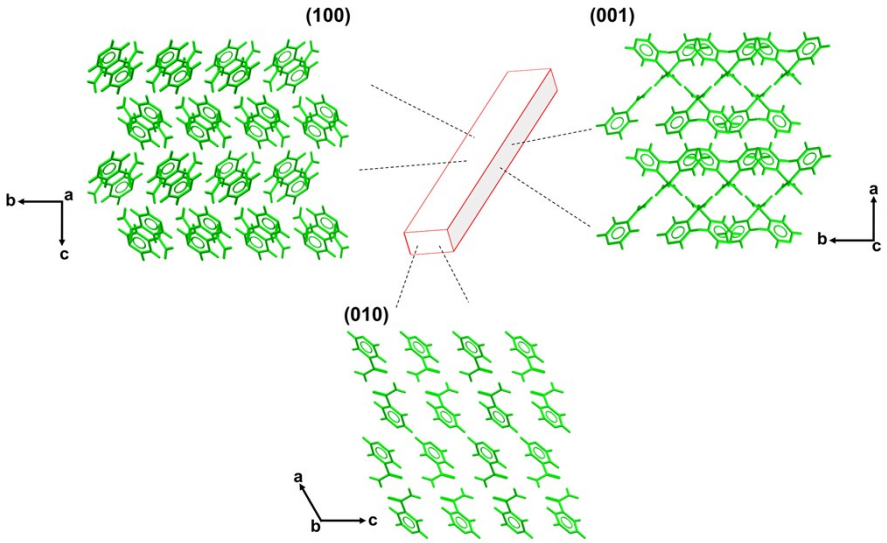

Figure S3. Molecular arrangements viewed along the different crystal faces and growth morphologies of the acicular form **I** crystals. The meanings of different colors are the same as those of Figure 3.

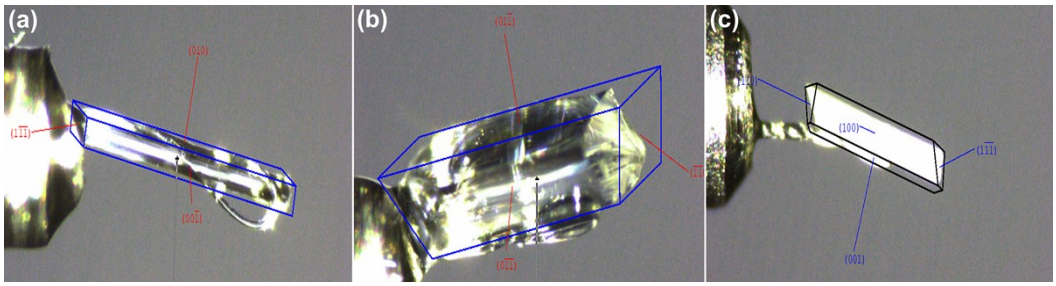

Figure S4. Face indexing measurements of the (a) acicular crystal and (b) rod-like crystal of INA form **H**, (c) and acicular crystal of form **I** (obtained at 0% RH).

2.4. Bending experiment

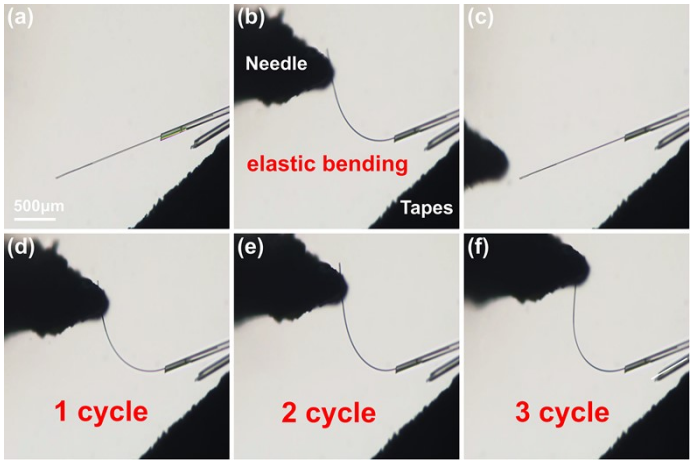

Figure S5. Optical microscopic photographs of an acicular single crystal of form **H** undergoing in-plane elastic bending for many times.

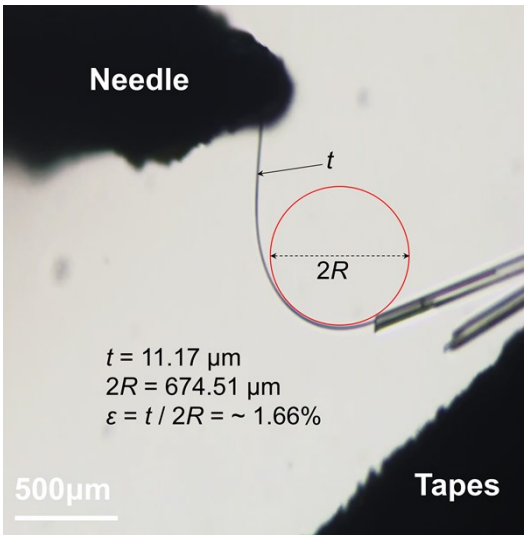

Figure S6. Elastic bending strain calculation of the acicular single crystal of INA form **H**.

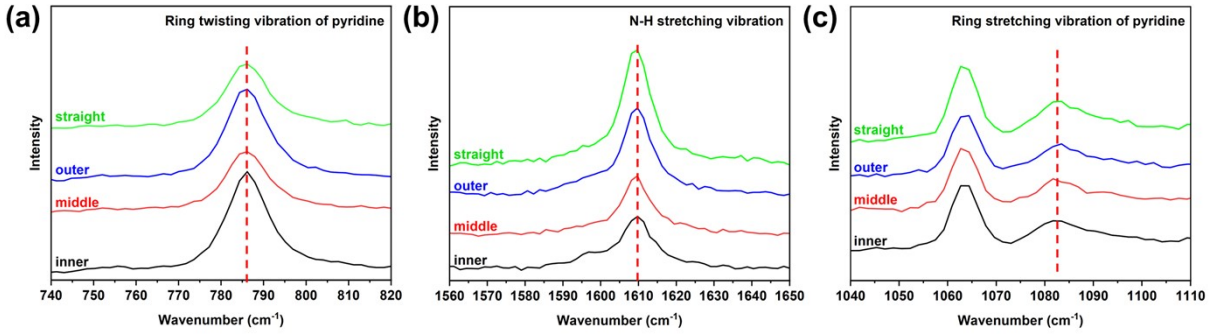

Figure S7. Experimental local Raman spectra of initially straight and bent crystals of acicular (a, b) INA form **H** and (c) form **I** (obtained at 0% RH).

2.5. Multi-stimuli-induced behaviors and SEM images

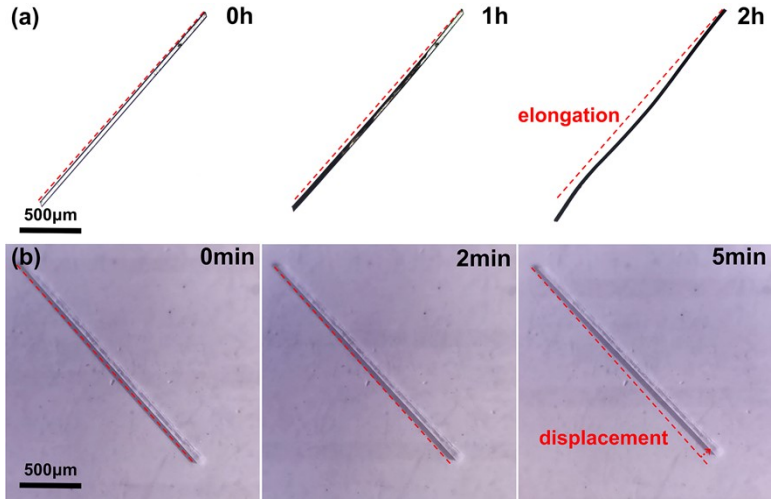

Figure S8. The microscopy images showing the phase transition process of (a) acicular form **H** → form **I** at 0% RH accompanied by elongation, and (b) acicular form **H** → form **II** at 50 °C accompanied by displacement.

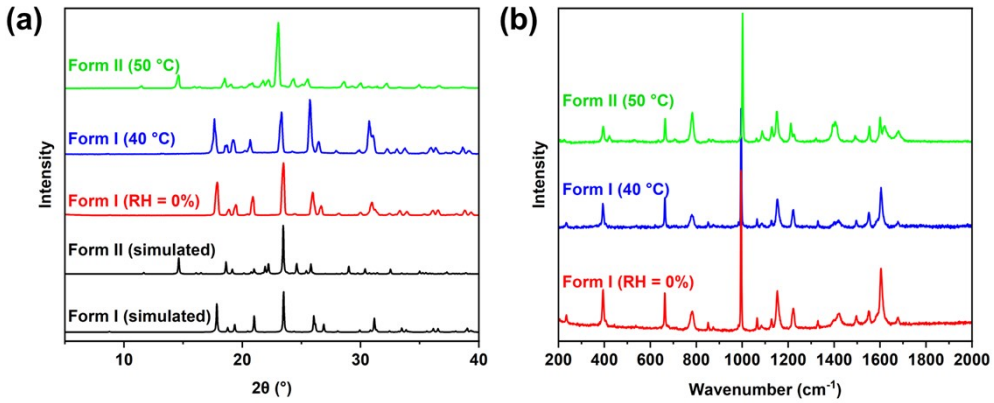

Figure S9. (a) PXRD patterns and (b) Raman spectra of form **I** and form **II** crystals obtained from phase transitions.

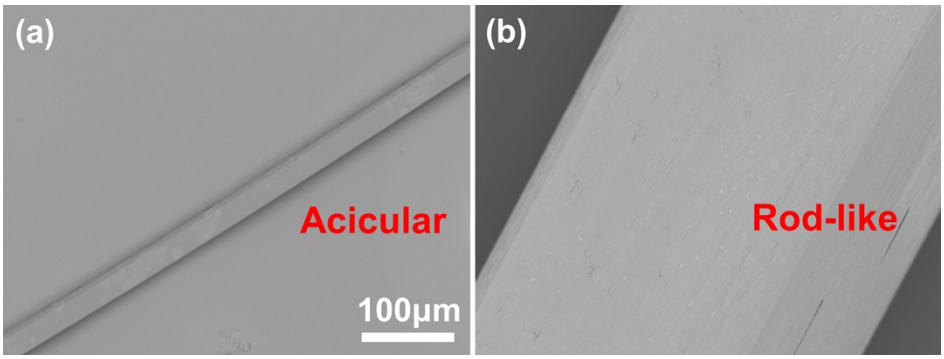

Figure S10. The SEM images of an (a) acicular and (b) rod-like crystal of form **H**.

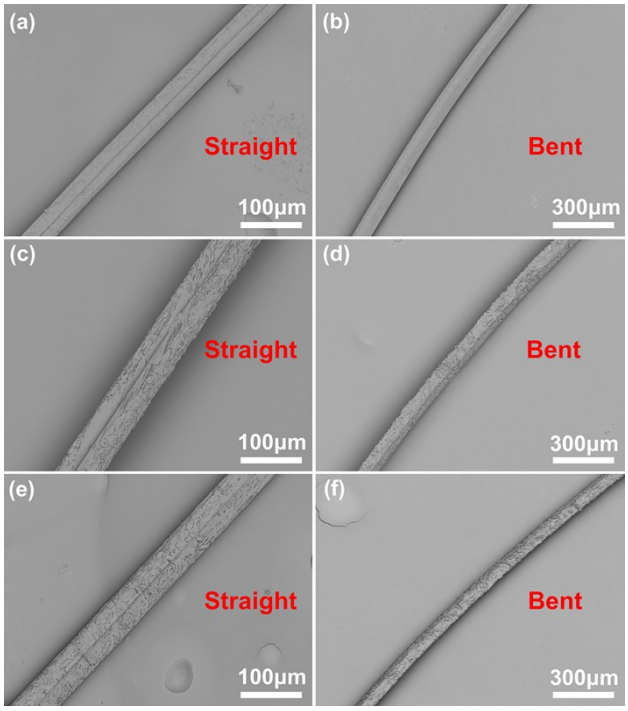

Figure S11. The SEM images of form **I** straight crystals obtained by (a) drying and (c) heating, (e) form **II** obtained by heating. (b, d, f) According mechanically bent cystals were also shown here.

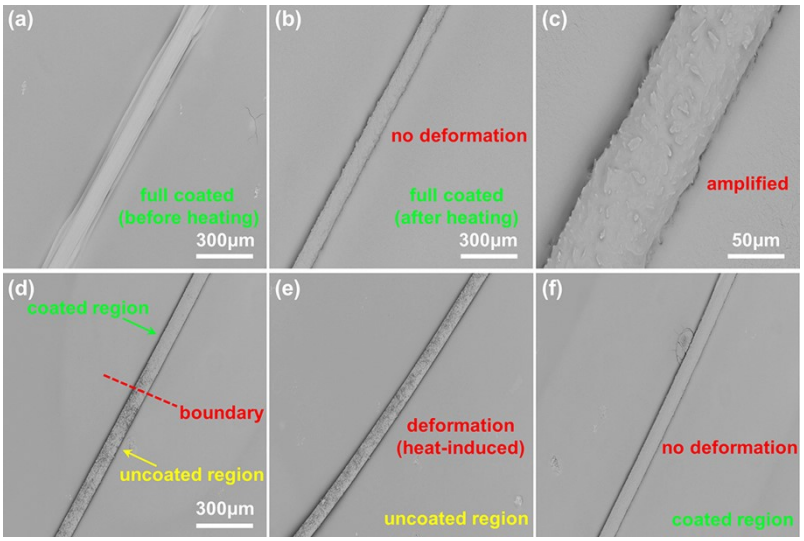

Figure S12. The SEM images of acicular form **H** crystals which were fully coated by silicone grease (a) before and (b, c) after heating at 50 °C without any deformation, and (d-f) half coated after heating at 50 °C along with deformation only in the uncoated region.

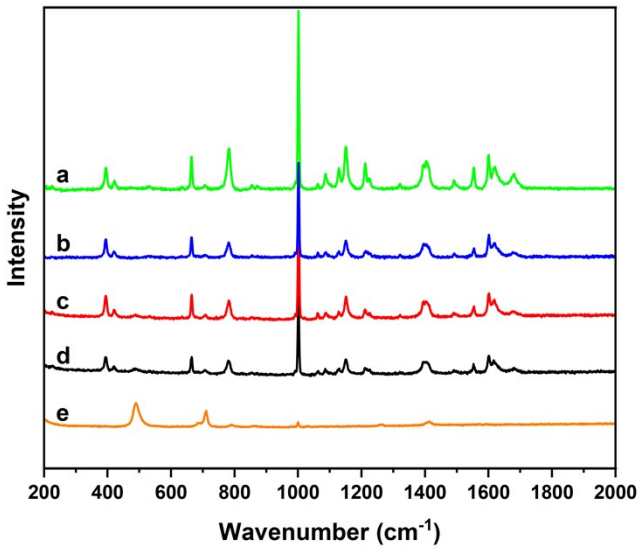

Figure S13. The Raman spectra of (a) uncoated and (d) full coated acicular crystals of form **H** upon heating at 50 °C after three days, and half coated crystal upon heating at 50 °C after three days in the case of the laser shining on the (b) exposed uncoated and (c) coated region respectively. (e) The Raman spectra of pure vacuum silicone grease.

2.6. Energy framework calculations

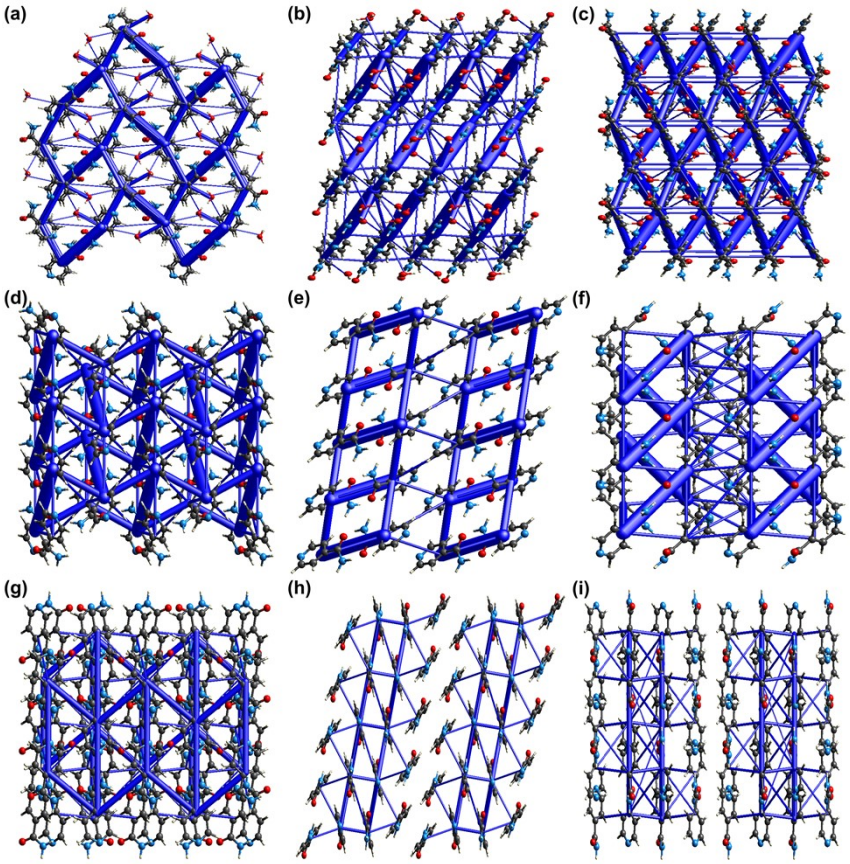

Figure S14. Calculated energy frameworks of INA (a-c) forms **H**, (d-f) **I** and (g-i) **II** in the different directions. Thicker tubes represent relatively stronger interactions. Frameworks are shown at an energy cut-off of 5 kJ mol^{-1} and tube size of 100.

Table S3. Details of interaction energy calculations in CrystalExplorer17.5.

Form H

	N	Symop	R	Electron Density	E_ele	E_pol	E_dis	E_rep	E_tot
	0	-	3.77	B3LYP/6-31G(d,p)	4.0	-2.8	-32.0	20.1	-13.3
	0	-x+1/2, y+1/2, -z+1/2	6.43	B3LYP/6-31G(d,p)	-0.1	-1.7	-10.3	5.3	-7.0
	1	-	7.58	B3LYP/6-31G(d,p)	-75.2	-16.0	-11.3	60.4	-63.9
	1	-	3.69	B3LYP/6-31G(d,p)	5.3	-2.2	-34.0	22.3	-11.8
	1	-	6.50	B3LYP/6-31G(d,p)	-37.0	-9.7	-16.5	44.5	-33.1
	0	-x, -y, -z	7.53	B3LYP/6-31G(d,p)	-8.3	-1.1	-5.0	0.7	-13.6
	0	-	7.10	B3LYP/6-31G(d,p)	4.1	-0.4	-0.9	0.1	3.3
	1	-	7.96	B3LYP/6-31G(d,p)	-4.2	-1.4	-3.4	2.1	-7.0
	1	-	6.56	B3LYP/6-31G(d,p)	-38.3	-9.9	-15.8	46.3	-33.1
	1	-	8.72	B3LYP/6-31G(d,p)	-2.5	-0.5	-1.4	0.1	-4.1
	0	-	4.10	B3LYP/6-31G(d,p)	-38.1	-8.8	-8.5	44.3	-26.9
	0	-	4.92	B3LYP/6-31G(d,p)	-5.7	-1.9	-5.0	7.2	-7.3
	0	-	4.50	B3LYP/6-31G(d,p)	5.2	-1.1	-5.2	3.1	2.1
	0	-	4.49	B3LYP/6-31G(d,p)	-5.8	-1.0	-5.6	6.3	-7.9
	0	-	5.08	B3LYP/6-31G(d,p)	-5.7	-1.1	-4.5	4.6	-7.9

Form I

	N	Symop	R	Electron Density	E_ele	E_pol	E_dis	E_rep	E_tot
	1	-x, -y, -z	5.17	B3LYP/6-31G(d,p)	-0.1	-0.9	-19.7	10.2	-11.6
	2	-x, y+1/2, -z+1/2	7.34	B3LYP/6-31G(d,p)	-9.0	-2.4	-9.1	12.9	-11.3
	1	-x, -y, -z	8.00	B3LYP/6-31G(d,p)	-7.5	-2.4	-8.3	9.4	-11.1
	0	-x, -y, -z	7.58	B3LYP/6-31G(d,p)	-71.3	-15.1	-11.1	58.4	-60.2
	1	x, y, z	5.73	B3LYP/6-31G(d,p)	-3.3	-1.3	-15.6	9.0	-12.5
	0	-x, y+1/2, -z+1/2	6.45	B3LYP/6-31G(d,p)	4.3	-1.7	-6.6	1.2	-1.7
	1	x, -y+1/2, z+1/2	5.59	B3LYP/6-31G(d,p)	-32.7	-8.6	-11.3	28.6	-33.1
	0	-x, -y, -z	5.38	B3LYP/6-31G(d,p)	-3.1	-2.5	-16.8	8.8	-14.3
	1	x, -y+1/2, z+1/2	5.97	B3LYP/6-31G(d,p)	0.4	-0.7	-11.3	8.8	-4.5

Form II

	N	Symop	R	Electron Density	E_ele	E_pol	E_dis	E_rep	E_tot
	1	-	4.85	B3LYP/6-31G(d,p)	-1.1	-1.9	-18.4	11.4	-11.5
	0	x, -y+1/2, z+1/2	6.62	B3LYP/6-31G(d,p)	-2.3	-0.6	-10.2	7.3	-7.2
	1	-	5.98	B3LYP/6-31G(d,p)	-1.6	-1.7	-9.6	3.4	-9.2
	0	x, y, z	8.02	B3LYP/6-31G(d,p)	-38.7	-9.3	-8.4	39.7	-30.7
	1	-	5.97	B3LYP/6-31G(d,p)	4.5	-1.5	-14.0	9.8	-2.4
	0	x, -y+1/2, z+1/2	6.14	B3LYP/6-31G(d,p)	-30.7	-9.0	-12.2	31.4	-30.3
	0	-x, y+1/2, -z+1/2	6.73	B3LYP/6-31G(d,p)	-5.9	-2.1	-8.5	6.6	-11.1
	0	-x, -y, -z	3.83	B3LYP/6-31G(d,p)	0.6	-1.0	-27.5	15.4	-14.5
	0	-x, -y, -z	8.53	B3LYP/6-31G(d,p)	-5.0	-0.4	-1.8	0.0	-7.1

2.7. Instructions of the supporting movies

Movie 1 shows the 2D elastic bending of acicular form **H** crystal.

Movie 5 shows the humidity-induced deformation of acicular form **H** crystal on drying at 0% RH.

Movies 8 shows the temperature-induced displacement of acicular form **H** crystal upon heating at 50 °C.

Movie 12 shows the elastoplasticity of acicular form **I** (obtained at 0% RH) crystals, which represents elastic and plastic bending in the different stage of mechanical bending.

3. References

(1) C. C. Seaton, A. Parkin, C. C. Wilson and N. Blagden, *Cryst. Growth Des*., 2009, **9**, 47-56.

(2) N. Fellah, C. J. Zhang, C. Chen, C. T. Hu, B. Kahr, M. D. Ward and A. G. Shtukenberg, *Cryst. Growth Des*., 2021, **21**, 4713-4724.

(3) O. V. Dolomanov, L. J. Bourhis, R. J. Gildea, J. A. K. Howard and H. Puschmann, *J. Appl. Crystallogr*., 2009, **42**, 339-341.

(4) G. M. Sheldrick, *Acta. Crystallogr. A. Found. Adv*., 2015, **71**, 3-8.

(5) G. M. Sheldrick, *Acta. Crystallogr. C. Struct. Chem*., 2015, **71**, 3-8.

(6) P. R. Spackman, M. J. Turner, J. J. McKinnon, S. K. Wolff, D. J. Grimwood, D. Jayatilaka and M. A. Spackman, *J. Appl. Crystallogr*., 2021, **54**, 1006-1011.